Biosynthetic electronic interfaces for bridging microbial and inorganic electron transport

*Leo (Huan-Hsuan) Hsu,⊥ Yixin Zhang,⊥ Pu Deng, Xiaochuan Dai and Xiaocheng Jiang**

Department of Biomedical Engineering, Tufts University, Medford, Massachusetts 02155, USA

ABSTRACT

Electron transport in biological and inorganic systems is mediated through distinct mechanisms and pathways. Their fundamental mismatch in structural and thermodynamic properties has imposed significant challenge on the effective coupling at the biotic/abiotic interface, which is central to the design and development of bioelectronic devices and their translation towards various engineering applications. Using electrochemically active bacteria, such as *G. sulfurreducens*, as a model system, here we report a bottom-up, bio-synthetic approach to synergize the electron transport and significantly enhance the coupling at the heterogeneous junction. In particular, graphene oxide was exploited as the respiratory electron acceptors, which can be directly reduced by *G. sulfurreducens* through extracellular electron transfer, closely coupled with outer membrane cytochromes in electroactive conformation, and actively "wire" the redox centers to external electrical contacts. Through this strategy, the contact resistance at the biofilm-electrode interface can be effectively reduced by 90%. Furthermore, the cyclic voltammetry reveals that the electron transfer of DL-1 biofilm transformed from a low-current (~0.36 μA), rate-limited profile to a high-current (~5μA), diffusion-limited profile. These results suggested that the integration of rGO can minimize the charge transfer barriers at the biofilm-

electrode interface. The more transparent contact at DL-1/electrode interface also enables unambiguous characterization of the inherent electron transport kinetics across the electroactive biofilm independent of cell-electrode interactions. The current work represents a strategically new approach toward the seamless integration of biological and artificial electronics, which is expected to provide critical insights into the fundamentals of biological electron transport and open up new opportunities for applications in biosensing, biocomputing and bioenergy conversion.

KEYWORDS

Extracellular electron transfer / graphene oxide / bio-reduction / electron hopping / biofilm

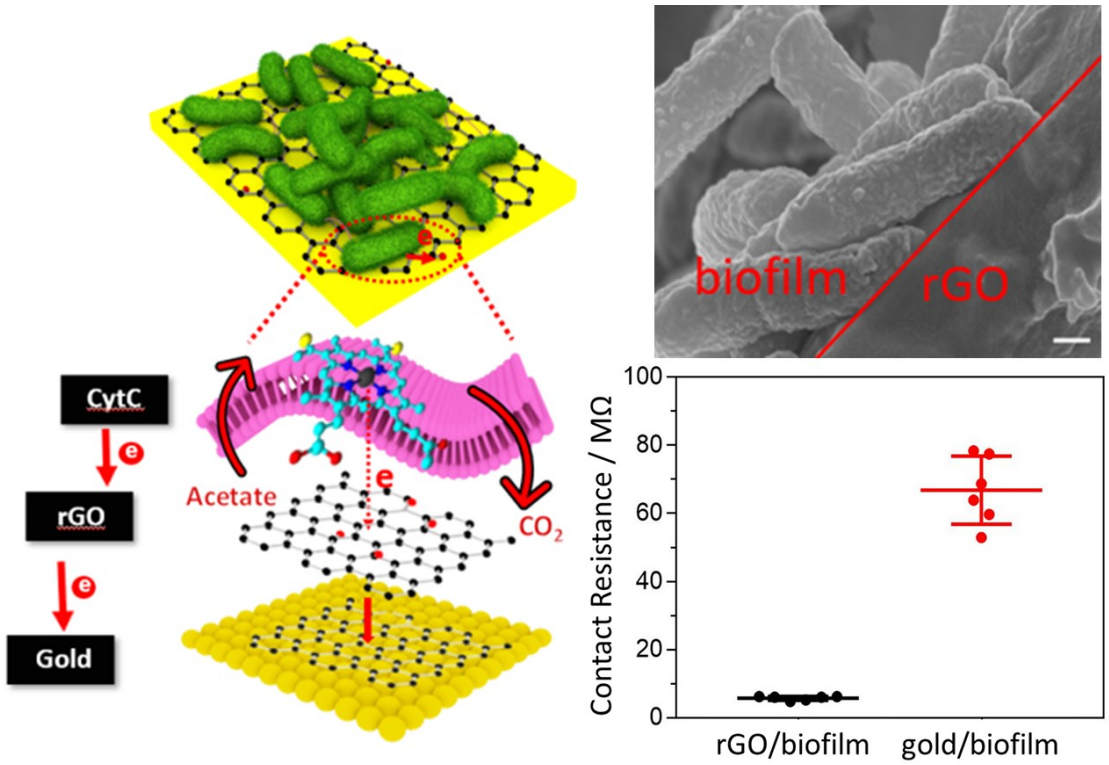

MAIN TEXT

Life is driven by the controlled flow of electrons. From photosynthesis to cellular respiration, redox electron transfers represent critical processes upon which many essential biological functions depend. The recent development of various bioelectronic interfaces and devices opens up unique opportunities to precisely interrogate and direct these biologically significant processes and is transforming pertinent research in both fundamental and translational territories.[1–4] The seamless structural and functional integration between biological and electronic components, however, remains challenging, mostly due to the compromised charge transport across the biotic-abiotic interface. Mediated through electron tunnelling or hopping (effective range of few nanometers),[5] the interfacial electrical coupling is strongly dependent on the distance between inorganic electrode and redox active centers. From a perspective of chemistry, these redox centers are usually buried deep inside of the insulating protein matrices and physically separated from external electrode. Their exposure, typically regulated by protein conformations, is sensitive to the microenvironments such as temperature, ionic strength, water contains and pH, thus further restricting the stability and reliability of electrical coupling. From a perspective of thermodynamics, the highly mismatched electronic structure/energy level between inorganic and biological surfaces typically results in contact barrier and low charge transfer rate at the hetero-junctions.[6]

A variety of approaches have been developed to enhance the electrical interconnection at bio-interfaces, including direct conjugation with redox cofactors to reduce the tunneling/hopping distance,[7,8] or utilization of molecular electron mediators to facilitate the charge transfer through intermediate redox reactions.[9,10] However, these methods are either too invasive (affecting protein conformations and activities) or lack of sufficient charge transfer rate to match the biological systems.[11] The recent advancement in nanomaterial design and synthesis brings forth new

possibility for bioelectrical interfacing as a result of their comparable dimension to biological building blocks and tunable electrical properties. Metal nanoparticles and carbon nanotube, for example, have been exploited to facilitate the electrical coupling with redox enzymes (e.g. glucose oxidase) by forming minimally invasive, nanoscale electrical linkage with redox centers,[12,13] yet challenges remain toward their effective bio-integration under dynamic conditions, especially when more complex biological machineries, such as functional organelles or whole cells, are involved.

Different from these traditional approaches where the primary focus has been on the "passive" electrode design/engineering, here we present a new strategy for "active" bio-interfacing by exploiting bio-initiated processes to construct synthetic electron conduits that naturally bridge biological and electrical circuits (**Figure 1a**). Electrochemically active bacteria (EABs) are known for their unique capability to electrically interact with external electron acceptors through extracellular electron transfer, which could create unique material interfaces, e.g., from dissimilatory reduction/biogenic production of inorganic nanoparticles, to potentially enhance the cross-system coupling.[14–17] While EABs can also directly "respire" electrodes through outer membrane cytochromes, the quality and reliability of the electrical contact is still far from optimal. In-situ nanoelectronic investigation of grown DL-1 biofilms showed that the two-terminal current is independent of the pair electrode distance but only related to electrode area, indicating that the electrical conduction across the biofilm is dominated by electrochemical electron transfer at the cell/electrode interface.[18] We have also carried out four-probe measurement on dried DL-1 biofilms to quantitatively assess the contact resistance, which appears to be 60 times larger than the intrinsic biofilm resistance (**Figure 1b**). Both results are suggesting the strong need to improve the interfacial electron transport, which can be achieved by designing and directing the

dissimilatory reduction of nanoscale electron acceptors to actively wire the redox active center of outer membrane cytochromes.

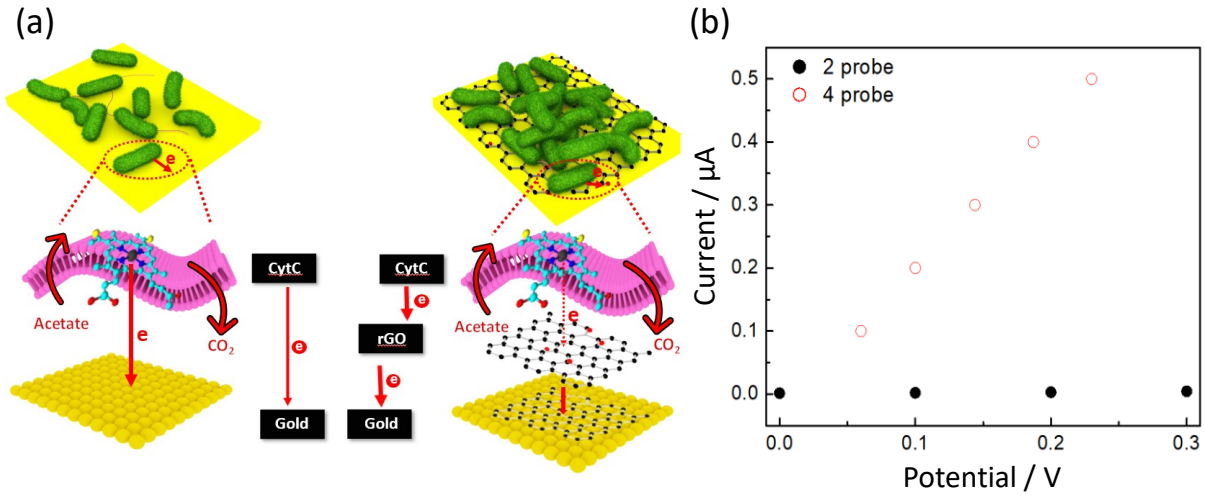

Figure 1. Reduced graphene oxide mediated charge transfers at gold/G. *sulfurreducens* DL-1 interfaces**.** (a). Schematic of DL-1 charge transfers on bare- and reduced graphene oxide covered- gold electrodes. The bio-reduced rGO was seamlessly coupled with the cytochrome C on the outer membranes of DL-1; thus, can effectively mediate the charge transfers between DL-1 and golds. (b). Two (black dots) and four probes (red circles) I-V measurements of DL-1 biofilm on gold electrodes. (applied potential: 0 to 0.3V). Resistances of each system were calculated by the slope of the regression line of each data as two probes: 78.7 MΩ and four probes: 0.43 MΩ. The contact resistance at DL-1/gold interface was derived by the difference of these two measurements.

For current studies, graphene oxide (GO) is selected as the terminal electron acceptors, which has been reported to be reducible under room temperature by a variety of EABs.[19,20] The bio-reduction process converts GO into reduced GO (rGO), as indicated by both color changes (from grayish to dark black color) (**Figure S1a**) and 5 order of magnitude increase of electrical conductance (from 1 nS to 698 μS) (**Figure S1b**). The transformation is further confirmed by Raman spectroscopy that characterizes the D and G bands originating from the in-phase vibration of the graphite lattice. A red-shift of the G-band, from 1598 to 1591 cm^{-1} (Figure S2), is observed after bio-reduction, consistent with the conversion from GO to rGO.[20] The intensity ratio between D and G bands (I_D/I_G), however, increases as a result of DL-1 doping and more out-of-plane sp3 bonds in the

hybrid material.[21] More critically, we hypothesize that the active reduction process will promote the physical contact and electrical coupling between the two distinct carbon-based charge transport systems with favorable conformations. To verify the hypothesis, we have fabricated arrays of gold microelectrodes with and without GO coating (**Figure 2a**).[22] A thin layer of GO film is selectively deposited onto electrodes following the lithography process, which smoothly covers the gold surface with minimal roughness change as revealed by the top- (Figure S3) and side-view SEM images (Figure S4). No detectable current is observed when ±1V bias is applied between the GO-covered source- and drain- electrodes, demonstrating the lack of direct electrical interconnection potentially contributed by residual GO in the electrode gap. The spatial specificity of GO deposition is also confirmed by high-magnification SEM imaging that shows sharp electrode interface with clean, GO free substrate (Figure S4). Based on these devices, systematic electrical and electrochemical characterizations were performed to investigate the effect of biologically reduced GO on interfacial charge transfer. First, two and four probe resistance measurements were carried out on DL-1 biofilms grown on top of rGO covered (rGO/biofilm) and bare gold (gold/biofilm) electrode after thorough wash and dehydration.[23] In both measurements, each current (two-probe) or voltage (four-probe) reading was recorded at the steady-state after allowing the exponential decay of the transient ion-induced responses from the liquid contain at the biofilm-electrode interfaces. Similar to previous measurements,[24] the I-V curves feature an almost linear response within the small bias regime, from which we can extract the 2-probe and 4-probe resistance values that respectively correspond to the whole system (biofilm+contact) and biofilm only (**Figure 2b**). As obtained contact resistance is on the order of tens of megaohm for biofilm/Au interface, with a large variation between different devices (50-80 MΩ; **Figure 2c**, red**).** This value can be significantly reduced to ~5.7± 0.5 MΩ when mediated through the biosynthesized rGO

(**Figure 2c**, black), indicating the formation of much more transparent and reliable electrical contact with DL-1 as compared with bare gold electrodes.

We attribute the improved contact transparency to the more effective structural and functional coupling as enabled by the active bioreduction process. As revealed by the high-resolution images

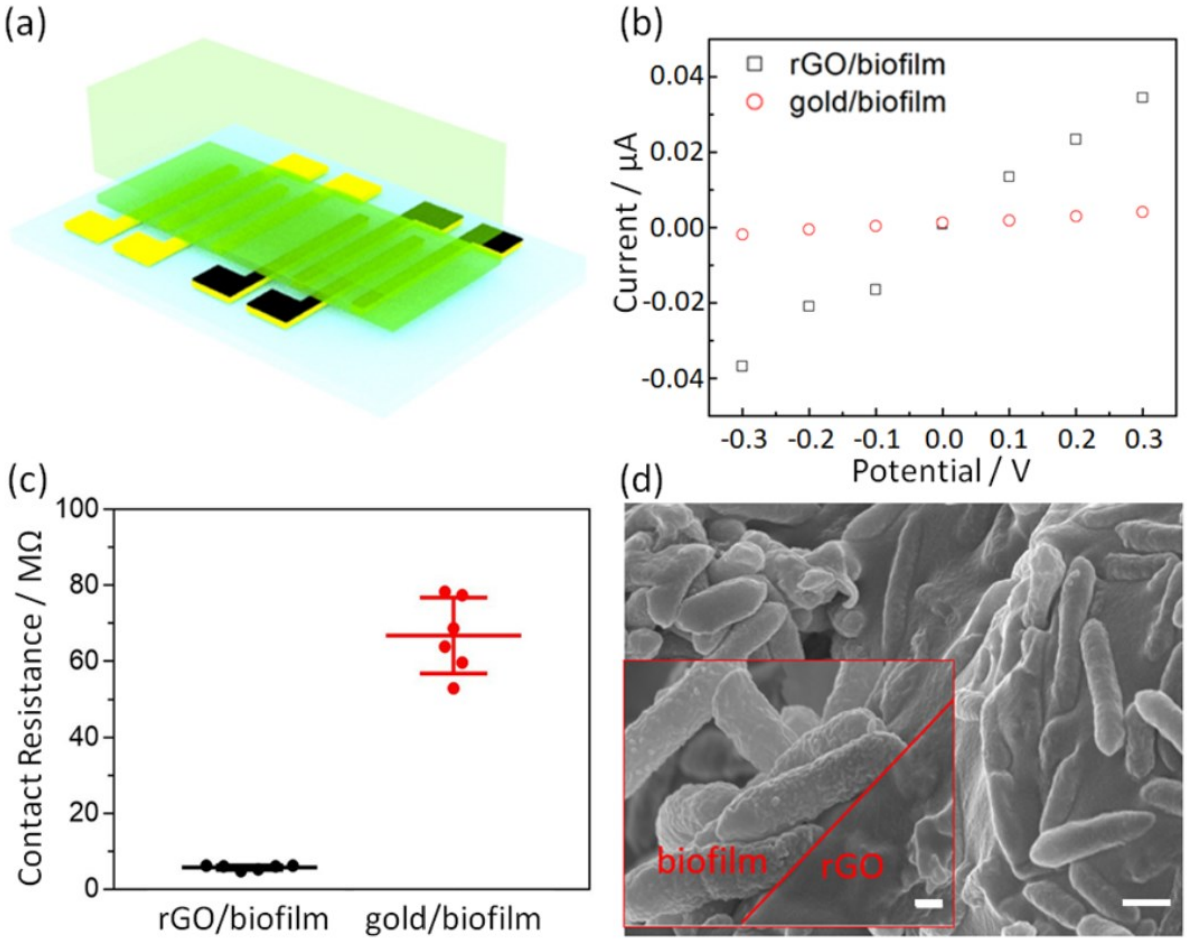

Figure 2. Effects of rGO in the charge transfers at DL-1/gold interfaces. (a) Schematic of the device. In the device, DL-1 biofilm was grown on both bare gold (yellow) and graphene oxide covered (black) electrodes covered by a single anaerobic chamber. The wide of each electrode is 1 mm, while the gap distance between two nearby electrodes is 1.5 mm. (b) measured currents of the rGO/biofilm (black squares) and gold/biofilm (red circles) under potential changes between -0.3 to 0.3 V. (c) Contact resistances of rGO/biofilm (black dots) and gold/biofilm (red dots) calculated from the two- and four- probe measurements. Row data is presented in Table S1. Error bars were calculated by the standard errors of 6 independent devices. (c). (d) SEM images of rGO/gold interface. The scale bar is 200 nm (inset) and 500 nm, respectively. The red line in the inset describes the interface boundary between the biofilm and rGO.

from scanning electron microscope (**Figure 2d**), the rGO is fully blended with DL-1 cells after the reduction/biomineralization, and the formed hybrids provide a seamless interface to the native biofilm. Previous molecular level studies suggested that at the electrode-protein interface, the rGO can induce conformational changes of the outermembrane cytCs that (i) expose extra redox cofactors to rGO that are commonly inaccessible[25,26] and (ii) reduce the distance between rGO and redox cofactors;[27] thus, elevate the charge transfer efficiency between electrode and cytCs. Moreover, the rGO enabled strong π-π interactions with cytC which can further promote electron hopping as well as physical adhesion.[28] These unique rGO-cytCs interplays actively wired the charge transfers between DL-1 and gold, which leads to significant reduction of contact resistance.

Charge transfers of the DL-1 biofilm involved both ionic supported, redox driven electron transfer (ET), and tunneling-based intermolecular electron transport (ETp).[5] To quantitatively investigate the interfacial ET, three-electrode cyclic voltammetry (CV) measurements[29] are carried out in fresh culture media without soluble electron donor/acceptor to eliminate the interference from DL-1 metabolism. Voltammograms from both GO-covered and bare gold electrodes show redox activities attributable to the outermembrane cytCs of DL-1 biofilms (oxidation potential of around -0.3V and reduction potential of around -0.45 V v.s. Ag/AgCl).[30] These results suggest that the introduction of rGO did not alter the mechanisms of redox-driven ETs in cytCs-based networks. However, the difference in CV profiles between gold/biofilm and rGO/biofilm indicated that the rGO can greatly improve the ET kinetics at the biointerface (**Figure 3a**). In gold/biofilm, the low-current (± 0.36 μA), rate-limited (sigmoid-shaped) ET profiles in both positive (cytC oxidation, ET from biofilm to gold) and negative (cytC reduction, ET from gold to biofilm) scans were led by the insufficient gold-cytC electrical coupling. In contrast, rGO/biofilm presented well-defined redox peaks of cytCs with enhanced current levels (± 5μA), consistent with faster, diffusion-

limited ET process. To exclude the possibility that the larger current was associated with the increase of effective electrode area after GO coating/reduction, we have performed control CV tests on both electrodes in 10 mM ferricyanide after removing biofilms. Comparable current magnitudes were observed in the CV scans, indicating that the surface area change caused by rGO coating is negligible (**Figure 3b**), which is consistent with the SEM characterizations (Figure S4). Instead, we attribute the transformation in ET kinetics to the increased density of redox active cytCs as a result of more effective linkage through the bioreductive process. It's also worth noting that the standard redox potential ($E_{1/2}$) of cytCs was shifted from -0.3 V to -0.24 V with the presence of rGO, indicative of protein conformational changes that can further facilitate the redox reactions of cytCs[25,26] Overall, the ET kinetics at biofilm-electrode interface was significantly

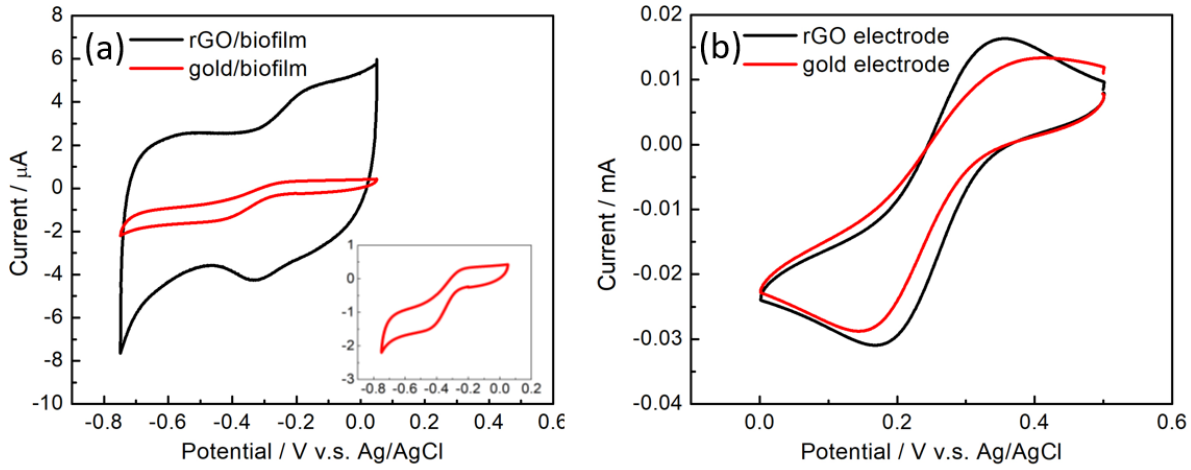

Figure 3. Electrochemical characterizations of rGO/biofilm and gold/biofilm. (a) Cyclic voltammetry of rGO/biofilm and gold/biofilm. The black and red curves represent electron transfer currents at the rGO/biofilm and gold/biofilm interfaces, respectively. (electrolyte: bacteria culture media; applied potential: -0.8 to 0 V; scan rate: 10 mV/s). (b) Cyclic voltammetry of electrochemically active surface areas of both rGO covered, and pure gold electrodes (electrolyte: potassium ferricyanide (10 mM); applied potential: 0 to 0.5V scan rate: 10 mV/s).

improved by creating structural and functional synergy from the bioreductive process, which actively coordinates the interfacial electron transport between rGO and DL-1 network and

significantly enhances the efficiency of translating metabolic processing into detectable electrical signals.

To fully decipher the ETp phenomenon in temporal domain, we have carried additional two-terminal measurements on washed & dehydrated devices[22] with either DC or AC inputs. For DC measurements, continuous potential sweeping is applied between ±1V with various scan rates to provide insight about charge transport under non-equilibrium conditions. For gold/biofilm, the source-drain current is minimal (< 0.5 nA) at low bias regime and shows exponential increase when the applied voltage is over ±0.4 V (red curve in **Figure 4a**). The tunneling barrier at small bias could be originating from non-optimal cytCs conformation/electrical contact, which could be overcome when the source-drain potential is raised above 0.4 V, bringing the HOMO-LUMO of cytCs and golds into resonance.[31] To better illustrate the interfacial tunneling barrier at gold/biofilm, the I-V characteristics are re-plotted as $\ln(I/V^2)$ vs. 1/V. The transition from logarithmic growth to linear decay at threshold voltage can be clearly observed for bare gold contact, thus further confirming the presence of contact barrier that limits charge transfer (**Figure S5**). In comparison, the measurement from rGO/biofilm sample shows much larger current without noticeable evidence for contact barrier within the measured voltage range (black curve in **Figure 4a**). Instead, substantial hysteresis, indicative of charge trapping, has been recorded during voltage sweeping, and becomes more significant with the increase of scanning rate. We believe this capacitive effect is associated with the detained electron transport across the biofilm as a result of additional electrostatic energy barrier when supporting electrolytes/counter ions are removed (thus reduced charge screening). This behavior could be obscured by the non-optimal contact/slow ETp rate across the contact barrier, and only becomes prominent when the interfacial electron transport is no longer a limiting factor. These results further demonstrate the potential of our strategy to

interrogate the intrinsic ETp properties of electroactive biofilms as well as other biological charge transport systems.

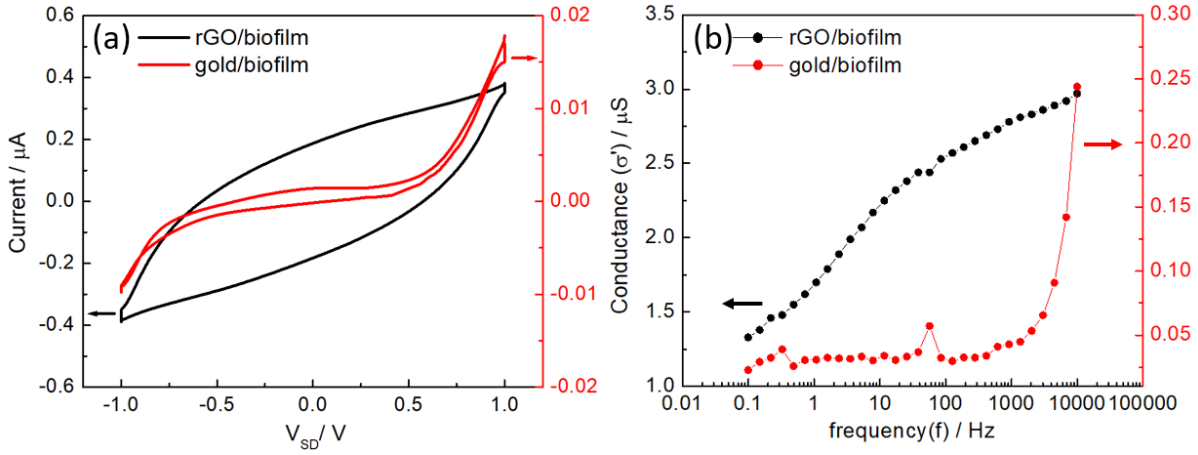

Figure 4. Cross biofilm electron transport measurements of rGO/biofilm and gold/biofilm of (a) DC inputs, the black and red curves represent the source-drain currents of rGO/biofilm and gold/biofilm, respectively (sweep between ±1 V, scan rate: 80 mV/s); (b) AC inputs, the black and red curves represent frequency-dependent impedances of rGO/biofilm and gold/biofilm, respectively. (applied bias: 0V, frequency: 0.1-10^4 (Hz)).

The two-terminal AC measurements were also conducted to investigate their frequency dependent response. For bare gold contact, the AC conductance of the DL-1 biofilm is composed of a low-frequency plateau and a dispersive high-frequency region with the critical frequency at 1000 Hz (red curve in **Figure 4b**), which can be modeled as a parallel resistance and capacity circuit.[32,33] At low frequency, ETp is restricted by the interfacial energy barrier as discussed in the DC measurement. When applying frequency above critical point, the electrical field induce extra energy to overcome the barrier that contribute to the dramatic increase of AC conductance. For rGO mediated contact, the AC conductance (σ'(ω)) of the biofilm exhibits almost linear frequency dependence. The σ'(ω) of rGO/biofilm can be expressed by the electron hopping model of conductive polymers/amorphous semiconductors and described as $\sigma'(\omega) = A\omega^s$(e.q 1),[34] where ω is the applied frequency, A is a temperature-dependent parameter, and s is correlated to energy barriers between two redox sites with a defined range between 0 to 1.[34] Since redox proteins are

randomly embedded in DL-1 biofilm, the energy barriers (value of *s*) between each redox protein pair can vary in a wide range during the charge transfer process. Each energy barrier can contribute a step-like profile in the AC conductance.[35] Hence, the overall AC conductance profile across the biofilm can be described as the overlap of these step-like profiles which results in the smooth AC conductance envelope with changing slopes (s) (black curve in **Figure 4b**).[35] Overall, these AC conductance measurements suggested that the ETp across our DL-1 biofilms is a hopping-driven process. While without rGO, charge transfer is dominated by the gold-biofilm interface which limits the ETp efficiency of the whole system.

To investigate the effect of rGO wiring on "solid-state" charge transport, we also performed electrical measurement after completely removing the tightly bound water molecules (i.e water inconveniently bonded with protein and water absorbed at the protein's surface) through solvent exchange and critical point drying.[36] Much lower current magnitude has been observed for both gold/biofilm and rGO/biofilm samples, comprising only 1-5% of the values from previous measurements (**Figure S6**). The results agree with molecular level studies which show the importance of tightly bound water in maintaining the protein structures involved in charge transport.[37] The removal of the tightly bound water also affects the quality of electrical contact, which seems to become more critical in solid-state transport. Only <50% of the Au/biofilm device give measurable current under our settings (i.e., I_{sd} >10 fA at 10V), which can be improved to >90% with the introduction of rGO at the interface. Among the measurable devices, the average current amplitude is also 10 times higher in rGO mediated devices, demonstrating the important role of rGO in enhancing the interfacial structural and/or electrical coupling in solid-state charge transport, which could open up new opportunities in translating these naturally derived functional materials/devices toward practical engineering applications.

In conclusion, taking advantage of the active bio-reduction of GO, we demonstrated the possibility to seamless merge the microbial and inorganic electron transport. These biosynthetic materials interface significantly enhanced both the ionically coupled ET and the solid state ETp processes at the gold-biofilm interface, which has been hindering the unambiguous understanding of the charge transfer mechanisms in biosystems and biotic-abiotic interfaces as well as the potential applications in bioelectronics. Moving forward, we believe this bio-synthetic strategy could be further extended to realize synergic bioelectronic interface with a broad range of biological charge transport systems at different structural and functional levels, including redox biomolecules (enzymes, chlorophyll, yeast etc.), functional organelles (mitochondria, chloroplast etc.), or wholes cells (EAB, cyanobacteria etc.). By bridging the gap between biological and electrical circuits, these efforts could evolve new capabilities to effectively interrogate and direct biologically significant processes, as well as novel bio-inspired systems/device concepts for a range of engineering applications.

ASSOCIATED CONTENTS

Supporting Information

Additional information including figures showing morphological/electrical characterization of DL-1/graphene oxide (GO) hybrids, Raman Spectrum of GO/rGO layer on electrode, SEM images of gold and GO coated gold electrodes, Fowler-Nordheim (FN) plots of two-terminal ETp, and solid-state ETp measurements after removing the tightly bound water molecules.

AUTHOR INFORMATION

Corresponding Author

*Email: Xiaocheng.Jiang@tufts.edu

Author Contributions

⊥Leo (Huan-Hsuan) Hsu and ⊥Yixin Zhang, contributed equally to this work.

Notes

The authors declare no competing financial interest.

ACKNOWLEDGMENT

The authors gratefully acknowledge support from National Science Foundation (NSF DMR-1652095) and Air Force Office of Scientific Research (FA9550-18-1-0128).

REFERENCES

(1) Wu, Y.; Hu, S. Biosensors Based on Direct Electron Transfer in Redox Proteins. *Microchim. Acta* **2007**, *159* (1), 1–17.

(2) Leech, D.; Kavanagh, P.; Schuhmann, W. Enzymatic Fuel Cells: Recent Progress. *Electrochim. Acta* **2012**, *84*, 223–234.

(3) Bhatnagar, D.; Xu, S.; Fischer, C.; Arechederra, R. L.; Minteer, S. D. Mitochondrial Biofuel Cells: Expanding Fuel Diversity to Amino Acids. *Phys. Chem. Chem. Phys.* **2011**, *13* (1), 86–92.

(4) Logan, B. E.; Hamelers, B.; Rozendal, R.; Schröder, U.; Keller, J.; Freguia, S.; Aelterman, P.; Verstraete, W.; Rabaey, K. Microbial Fuel Cells: Methodology and Technology. *Environ. Sci. Technol.* **2006**, *40* (17), 5181–5192.

(5) Bostick, C. D.; Mukhopadhyay, S.; Pecht, I.; Sheves, M.; Cahen, D.; Lederman, D. Protein Bioelectronics: A Review of What We Do and Do Not Know. *Reports Prog. Phys.* **2018**, *81* (2).

(6) Gallaway, J. W.; Calabrese Barton, S. A. Kinetics of Redox Polymer-Mediated Enzyme

Electrodes. *J. Am. Chem. Soc.* **2008**, *130* (26), 8527–8536.

(7) Calabrese Barton, S.; Gallaway, J.; Atanassov, P. Enzymatic Biofuel Cells for Implantable and Microscale Devices. *Chem. Rev.* **2004**, *104* (10), 4867–4886.

(8) Barrière, F.; Kavanagh, P.; Leech, D. A Laccase–glucose Oxidase Biofuel Cell Prototype Operating in a Physiological Buffer. *Electrochim. Acta* **2006**, *51* (24), 5187–5192.

(9) Lentini, R.; Santero, S. P.; Chizzolini, F.; Cecchi, D.; Fontana, J.; Marchioretto, M.; Del Bianco, C.; Terrell, J. L.; Spencer, A. C.; Martini, L.; et al. Integrating Artificial with Natural Cells to Translate Chemical Messages That Direct E. Coli Behaviour. *Nat. Commun.* **2014**, *5*, 4012.

(10) Chaubey, A.; Malhotra, B. D. Mediated Biosensors. *Biosens. Bioelectron.* **2002**, *17* (6), 441–456.

(11) Willner, I.; Katz, E. Integration of Layered Redox Proteins and Conductive Supports for Bioelectronic Applications. *Angew. Chemie Int. Ed.* **2000**, *39* (7), 1180–1218.

(12) Anthony, G.-E.; Chenghong, L.; Ray, H. B. Direct Electron Transfer of Glucose Oxidase on Carbon Nanotubes. *Nanotechnology* **2002**, *13* (5), 559.

(13) Willner, I.; Willner, B.; Katz, E. Biomolecule-Nanoparticle Hybrid Systems for Bioelectronic Applications. *Bioelectrochemistry* **2007**, *70* (1), 2–11.

(14) Narayanan, K. B.; Sakthivel, N. Biological Synthesis of Metal Nanoparticles by Microbes. *Adv. Colloid Interface Sci.* **2010**, *156* (1), 1–13.

(15) Thakkar, K. N.; Mhatre, S. S.; Parikh, R. Y. Biological Synthesis of Metallic Nanoparticles. *Nanomedicine Nanotechnology, Biol. Med.* **2010**, *6* (2), 257–262.

(16) Jiang, X.; Hu, J.; Lieber, A. M.; Jackan, C. S.; Biffinger, J. C.; Fitzgerald, L. A.; Ringeisen, B. R.; Lieber, C. M. Nanoparticle Facilitated Extracellular Electron Transfer in Microbial Fuel Cells. *Nano Lett.* **2014**, *14* (11), 6737–6742.

(17) Hsu, L.; Deng, P.; Zhang, Y.; Nguyen, H. N.; Jiang, X. Nanostructured Interfaces for Probing and Facilitating Extracellular Electron Transfer. *J. Mater. Chem. B* **2018**, *6* (44), 7144–7158.

(18) Ding, M.; Shiu, H. Y.; Li, S. L.; Lee, C. K.; Wang, G.; Wu, H.; Weiss, N. O.; Young, T. D.; Weiss, P. S.; Wong, G. C. L.; et al. Nanoelectronic Investigation Reveals the Electrochemical Basis of Electrical Conductivity in Shewanella and Geobacter. *ACS Nano* **2016**, *10* (11), 9919–9926.

(19) Salas, E. C.; Sun, Z.; Lüttge, A.; Tour, J. M. Reduction of Graphene Oxide via Bacterial Respiration. *ACS Nano* **2010**, *4* (8), 4852–4856.

(20) Wang, G.; Qian, F.; Saltikov, C. W.; Jiao, Y.; Li, Y. Microbial Reduction of Graphene Oxide by Shewanella. *Nano Res.* **2011**, *4* (6), 563–570.

(21) Kalathil, S.; Katuri, K. P.; Alazmi, A. S.; Pedireddy, S.; Kornienko, N.; Costa, P. M. F. J.; Saikaly, P. E. Bioinspired Synthesis of Reduced Graphene Oxide-Wrapped Geobacter Sulfurreducens as a Hybrid Electrocatalyst for Efficient Oxygen Evolution Reaction. *Chem. Mater.* **2019**, *31* (10), 3686–3693.

(22) Electrodes were fabricated using photo- or stencil-lithography on the glass substrates. For photolithography, S1813 was used as photoresist to define the electrode area following selected-area exposure and resist development. For stencil-lithography, Kapton tapes were applied as the shadow masks and patterned with laser cutter (electrode width: 1 mm; gap:

3 mm). Cr (10 nm)/Au (50 nm) film was then deposited on the glass substrates using thermal evaporator or sputter coater (NSC 3000 DC Magnetron Sputter Tool). To fabricate GO covered electrodes, a 0.4 wt% GO solution was drop-casted onto the substrate before removing the photoresist or Kapton tape, thoroughly washed by DI water to remove loosely bound GO, and dried using ethanol and hot plate baking at 60°C. After the electrode fabrication, the photoresist/ Kapton tapes were removed to expose the gaps between electrodes.

(23) *G.sulfurreducens* DL-1 were cultured based on ATCC protocol (https://www.atcc.org/products/all/51573.aspx#culturemethod). The biofilm was cultured in a chamber attached to the electrode which contained 3 ml culture media. This setup was purged with 80% N_2–20% CO_2 gas mixture during the whole culture period. After 3 days of culture, as formed DL-1 biofilm was fixed by 2% of glutaraldehyde solution for 30 minutes. Next, biofilm was washed 3 times by deionized water and then dehydrated with 100% ethanol before electrical measurements. In 2 probe measurements, the current was detected using a current amplifier (1211; DL Instruments, Inc.) with a gain of 10^9–10^{11} V/A. The amplified signals were digitized by a multichannel analogue-to-digital converter (USB-6341; National Instruments). The 4-probe measurement was performed by connecting outer two electrode with constant current source (C5580; Stanford Research Systems). The voltage across inner two electrodes was detected by a voltage amplifier (Brownlee Precision) and digitized using above mentioned multichannel analogue-to-digital converter. The contact resistance was calcualted by subtracting each individual 4-probe resistance from its corrsponed 2-probe resistance.

(24) Malvankar, N. S.; Vargas, M.; Nevin, K. P.; Franks, A. E.; Leang, C.; Kim, B.-C.; Inoue,

K.; Mester, T.; Covalla, S. F.; Johnson, J. P.; et al. Tunable Metallic-like Conductivity in Microbial Nanowire Networks. *Nat. Nanotechnol.* **2011**, *6* (9), 573–579.

(25) Zuo, X.; He, S.; Li, D.; Peng, C.; Huang, Q.; Song, S.; Fan, C. Graphene Oxide-Facilitated Electron Transfer of Metalloproteins at Electrode Surfaces. *Langmuir* **2010**, *26* (3), 1936–1939.

(26) Patila, M.; Pavlidis, I. V.; Diamanti, E. K.; Katapodis, P.; Gournis, D.; Stamatis, H. Enhancement of Cytochrome c Catalytic Behaviour by Affecting the Heme Environment Using Functionalized Carbon-Based Nanomaterials. *Process Biochem.* **2013**, *48* (7), 1010–1017.

(27) Zhao, D.; Li, L.; Zhou, J. Simulation Insight into the Cytochrome c Adsorption on Graphene and Graphene Oxide Surfaces. *Appl. Surf. Sci.* **2018**, *428*, 825–834.

(28) Zhang, Y.; Zhang, J.; Huang, X.; Zhou, X.; Wu, H.; Guo, S. Assembly of Graphene Oxide–Enzyme Conjugates through Hydrophobic Interaction. *Small* **2012**, *8* (1), 154–159.

(29) CV was performed by Biologic SP200 Potentiostat using a three-electrode configuration. The Ag/AgCl (3M KCl) was used as reference electrode, while the carbon cloth was used as counter electrode.

(30) Richter, H.; Nevin, K. P.; Jia, H.; Lowy, D. A.; Lovley, D. R.; Tender, L. M. Cyclic Voltammetry of Biofilms of Wild Type and Mutant Geobacter Sulfurreducens on Fuel Cell Anodes Indicates Possible Roles of OmcB, OmcZ, Type IV Pili, and Protons in Extracellular Electron Transfer. *Energy Environ. Sci.* **2009**, *2* (5), 506.

(31) Cui, X. D.; Zarate, X.; Tomfohr, J.; Sankey, O. F.; Primak, A.; Moore, A. L.; Moore, T.

A.; Gust, D.; Harris, G.; Lindsay, S. M. Making Electrical Contacts to Molecular Monolayers. *Nanotechnology* **2001**, *13* (1), 5–14.

(32) Gabrielli, C.; Haas, O.; Takenouti, H. Impedance Analysis of Electrodes Modified with a Reversible Redox Polymer Film. *J. Appl. Electrochem.* **1987**, *17* (1), 82–90.

(33) Musiani, M. M. Characterization of Electroactive Polymer Layers by Electrochemical Impedance Spectroscopy (EIS). *Electrochim. Acta* **1990**, *35* (10), 1665–1670.

(34) Tsonos, C. Comments on Frequency Dependent AC Conductivity in Polymeric Materials at Low Frequency Regime. *Curr. Appl. Phys.* **2019**, *19* (4), 491–497.

(35) Tsuji, K.; Han, H.; Guillemet-Fritsch, S.; Randall, C. A. Dielectric Relaxation and Localized Electron Hopping in Colossal Dielectric (Nb,In)-Doped TiO2 Rutile Nanoceramics. *Phys. Chem. Chem. Phys.* **2017**, *19* (12), 8568–8574.

(36) Both dehydrated samples are submerged in 100% ethanol inside the critical point dryer (Leica EM CPD300). Twenty cycles of critical point CO_2 exchanges with low exchange rate are applied to remove tightly bound water in biofilms.

(37) Ron, I.; Sepunaru, L.; Itzhakov, S.; Belenkova, T.; Friedman, N.; Pecht, I.; Sheves, M.; Cahen, D. Proteins as Electronic Materials: Electron Transport through Solid-State Protein Monolayer Junctions. *J. Am. Chem. Soc.* **2010**, *132* (12), 4131–4140.